Experimental band structure of lead

G. Jézéquel* and I. Pollini†
Laboratoire de Spectroscopie du Solide, Université de Rennes I, Campus de Beaulieu, 35042 Rennes CEDEX, France
(Received 15 March 1989; revised manuscript received 10 October 1989)

By using angle-resolved photoemission with synchrotron radiation, we have determined accurate energy-versus-momentum dispersion relations along symmetry lines ΓX and ΓKX for lead crystals. These directions are mapped out by recording normal-emission photoelectron spectra at low temperatures (20 K) from Pb(100) and Pb(110) surfaces, and by interpreting the experimental data in terms of the direct-transition model. However, in the photon-energy range 55–65 eV the photoemission curves for Pb(100) are best interpreted by taking into account the influence of inelastic electron scattering in the final state (momentum-nonconserving transitions). The experimental dispersion curves for the valence bands of p and s symmetry are in fine agreement with the theoretical electronic structure obtained by relativistic augmented–plane-wave (APW) and linear rigorous cellular (LRC) methods.

I. INTRODUCTION

Angle-resolved photoemission spectroscopy (ARPES), particularly when used in conjunction with polarized and tunable synchrotron radiation, allows one to measure the band structure of metals and semiconductors with high accuracy. Excellent results were obtained in the case of metals such as Cu,[1,2] Ag,[3] Au,[4] and Al,[5] and semiconductors such as GaAs (Ref. 6) and GaP.[7] All these results have been discussed within the framework of the direct-transition model,[2,8] which makes use of energy and momentum conservation principles. This model relies on the one-electron approximation which is strictly valid only for noninteracting electrons, at 0 K temperature. Besides, the conservation of the parallel component of the wave vector, $K_{\parallel}$, at the crossing of the surface is only valid if the crystal surface is ideal. These assumptions will be critically considered during the discussion of the experimental results.

Previous studies on lead were devoted to x-ray photoemission spectroscopy[9] (XPS), angle-integrated photoemission,[10] and, more recently, to ARPES applied to the Pb(111) face.[11]

The electronic level occupation in lead is $5d^{10}6s^26p^2$. The $5d^{10}$ core levels lie well below the Fermi level (-20 eV) so that only $6s$ and $6p$ states contribute to the occupied valence bands. The band structure of lead is then relatively simple and particularly interesting because relativistic effects (spin-orbit coupling, and Darwin and mass-velocity terms) manifest themselves in a clear manner. In the ΓX direction of the first Brillouin zone (BZ), the electronic structure consists of two bands: a full s band separated by a large gap(due in part to Darwin and mass-velocity terms) from a partially filled p band. Their overall shape is essentially free-electron-like. However, in the ΓKX direction, this description is modified for the p bands which are strongly affected by the spin-orbit interaction.[11] Thus, experimentally, it will be sufficient to determine the band energies at a few critical points in order to check whether or not band-structure calculations correctly describe its electronic structure. Band-structure calculations for Pb based on the relativistic augmented–plane-wave (RAPW) scheme,[12] the pseudopotential method,[13] and the linear combination of atomic orbitals (LCAO) approximation[14] are known and show in general good agreement with the available Fermi-surface data and XPS valence-band spectra.[14,15] More recently, a self-consistent relativistic linear rigorous cellular (LRC) method[11] has been used to calculate the band structure of bulk lead up to about 30 eV above the Fermi energy (E_F). This latter calculation makes use of the Hedin-Lundqvist approximation for the exchange interaction and correlation forces.[16]

A recent work by Jezequel *et al.*,[17] in which angle-resolved photoelectron spectra from Pb(110) were obtained at room and liquid-nitrogen temperatures, gives evidence that indirect transitions dominate the photoemission spectra of this surface at room temperature between 60 and 110 eV. Our results on Pb (100) (Ref. 17) and also Horn's[11] results on Pb(111) show that direct transitions may be observed at room temperature, at lower photon energies (the surface Debye temperature is also higher for these surfaces). However, those direct transitions are superposed on an indirect-transition contribution which might shift the energy location of the peaks.

To overcome these difficulties, this paper reports on the results of low-temperature measurements ($T=20$ or 77 K) of normal-emission ARPES spectra on Pb(100) and Pb(110), i.e., along ΓX and ΓKX high-symmetry directions of the BZ. The results are interpreted within the framework of the direct-transition model, except in the photon-energy range 55–67.5 eV for Pb(100) where hole and electron lifetimes are taken into account. Throughout the paper both $K_{\perp}$ and $k_{\perp}$ are used for the normal momentum: wave-vector symbols are then referred to the extended ($K_{\perp}$) and the reduced ($k_{\perp}$) Brillouin zone.

The experimental methods and results are described in Secs. II and III. In Sec. IV lifetime effects are considered.

A short account of this section was already given in Ref. 17. Section V presents the experimental dispersions for initial and final states and their comparison with band-structure calculations. Conclusions are drawn about the results in the final section.

II. EXPERIMENTAL METHODS

The photoemission experiments were performed at the Laboratoire pour l'Utilisation du Rayonnement Electromagnétique (LURE) at Orsay, France. Monochromatized synchrotron radiation from either a toroidal grating monochromator (photon energy $\hbar\omega > 30$ eV) or else a normal-incidence monochromator ($9 < \hbar\omega < 30$ eV) was used for photoexcitation. Spectra were obtained for photon energy between 9 and 120 eV with a combined resolution of the photon monochromator and electron spectrometer smaller than 250 meV for photon energies below 40 eV and ranging from 250 to 400 meV for energies between 40 and 100 eV. The measurements were performed with the light beam set at an angle of incidence of 67.5° (*p*-polarized light). The resolved electron distribution curves were recorded using a spherical photoelectron spectrometer with an angular resolution of $\pm 0.7°$

All single-crystal samples were cut from 99.999%-purity lead single-crystal bars. The bars were first oriented with Laue x-ray backscattering to within 1° of the desired orientation, and then approximately 2 mm × 10 mm disks were spark cut perpendicular to the desired axis. The faces were etched and chemically polished in a solution of 20% hydrogen peroxide (dilution: 30 volumes) and 80% glacial acetic acid. The polished samples were then glued to the cold end of a helium-flow cryostat attached to a part of a differentially pumped rotary motion. After the spectrometer was pumped by standard techniques to a basic pressure in the low 10^{-10} millibar range, the crystals were cleaned by argon-ion etching followed by annealing to 150°C to remove the disorder caused by the etching. The etching-annealing cycles were stopped when the surfaces displayed good (1×1) low-energy electron diffraction (LEED) patterns indicative of sufficient long-range order. No residual surface impurities were observed using Auger-electron spectroscopy: the surface cleanliness could be further checked by using the valence-band and core-level photoemission spectra of lead.

III. EXPERIMENTAL RESULTS

ARPES has become a common technique for the experimental determination of the three-dimensional bulk band structure of solids. The simplest method consists of recording the spectra in normal emission ($K_{\parallel}=0$) for a wide range of photon energies from a given crystallographic face. The normal component of the wave vector inside the crystal $K_{\perp}$ is not conserved when crossing the surface, because of the potential barrier at the surface. However, if the final-state dispersion is known, one can determine the wave vector $K_{\perp}$ corresponding to the transitions giving rise to photoemission peaks at any photon energies and thus obtain the experimental dispersion of the initial states. The usual approach is to assume that the final-state band structure can be described by a free-electron parabola: the bottom of the parabola (or equivalently V_0, the inner potential) and the effective mass are then used as adjustable parameters which are fitted to give the best agreement with the observed dispersion effects. We shall present now the most important experimental results for the faces Pb(100) and Pb (110).

A. Pb(100): High-symmetry line ΓX

Normal-emission low-temperature photoelectron spectra for photon energy between 35 and 100 eV are shown in Figs. 1 and 2. The photoemission peaks A and (B,B'), corresponding to valence bands of p and s symmetry, respectively, are separated by a gap over the whole spectral region under study. By considering the energy shifts of the photoemission structures as a function of the photon energy (vertical dashes on figures) one can draw Fig. 3.

In this figure we have plotted, for each structure (A,B,B'), the initial-state energy E_i versus the final-state energy $E_f=\hbar\omega-|E_i|$. All energies are referenced to the Fermi energy. Such a diagram allows us to obtain immediate information on the final-state dispersions and in particular on the location of the high-symmetry points. Peak A reaches the lowest value of the initial-state energy (binding energy), 3 eV below E_F, for $E_f=40$ and 52.5 eV, and approaches E_F around 33 and 68 eV. Peak B has a maximum of the binding energy (−7.15 eV) for $E_f=40$ and 52.5 eV, and then disperses down to −9 eV for $E_f=68$ eV. This peak reaches the minimum value of the binding energy (−11.4 eV) around $E_f=24.5$ eV. For both peaks (A and B), almost no dispersion is observed between 40 and 52 eV.

From the symmetry of the diagram giving the dispersion of peaks A and B one can conclude that both structures follow the same final-state band dispersions. Furthermore, from previous knowledge of the lead band structure,[12] one can make the following observations about the final band dispersions: (i) a final-state band $F1$ disperses from Γ to X between $E_f=24.5$ eV (Γ) and 40 eV (X); (ii) the observed peaks follow a second final band F_2 between 52.5 eV above E_F (X point) and 68 eV above E_F and then follow another final band F_3, before reaching the Γ point.

By considering, for example, the final-state energy of the s and p bands at the high-symmetry point X (52.5 eV), one observes that the dispersion of the unoccupied final band $F2$ can be tentatively described by the free-electron parabola:

$$E_f=\hbar(k_{\perp}-G_{002})^2/2m^*+V_0 \tag{1a}$$

with $V_0=-11.4$ eV and $m^*=0.88m$.

From the diagram of Fig. 3, connecting the initial (E_i) and final (E_f)-state energies, and from Eq. (1), which gives the relation between E_f and $k_{\perp}$, we at once obtain the experimental points of the valence-band structure in the direct-transition model. These results will be discussed in Sec. IV.

The dispersion along ΓX for the final bands $F1$ and $F3$ will be discussed in Sec. V B.

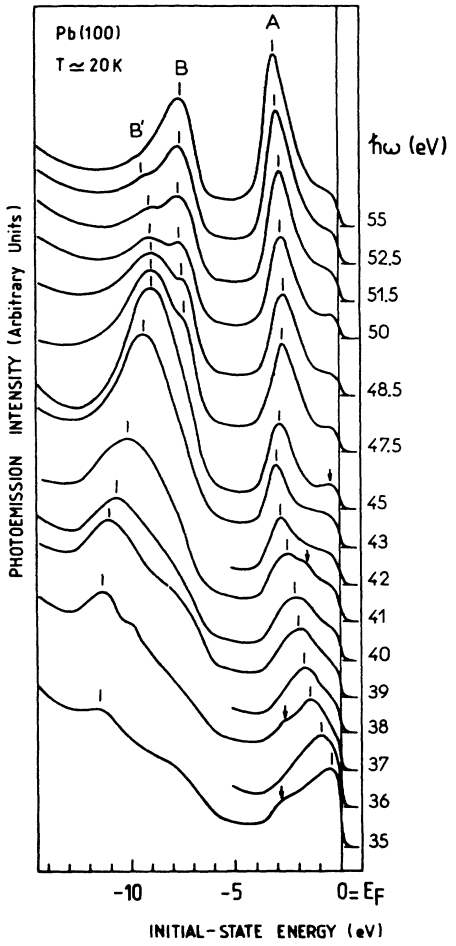

FIG. 1. Low-temperature ($T \simeq 20$ K) normal-emission photoelectron spectra plotted as a function of the binding energy for Pb (100), for incident photons of energy between 35 and 55 eV. Peaks A and B,B' are related to the experimental band dispersions of valence bands p and s, respectively.

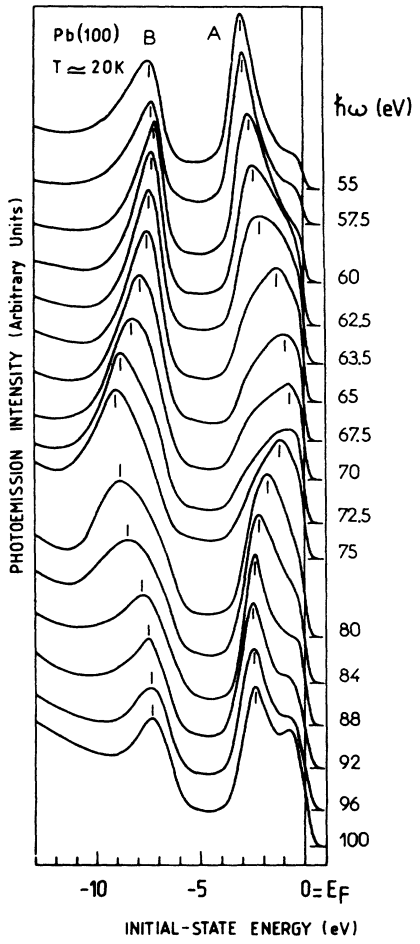

FIG. 2. Low-temperature ($T \simeq 20$ K) normal-emission photoelectron spectra for Pb(100) recorded for photon energies between 55 and 100 eV. Peaks A and B give the experimental dispersions of valence-band states p and s, respectively.

B. Pb(110): high-symmetry line ΓKX

Normal-emission spectra for a photon energy between 35 and 100 eV and $T=77$ K are shown in Figs. 4 and 5. Three photoemission peaks A, B, and C, corresponding to bands of symmetry p and s present in the ΓKX direction of the BZ, occur in the photon range 68–100 eV. Beyond 62 eV peak A (p-like) disperses very little, reaching a minimum value of the initial-state energy at 0.8 eV below E_F for $\hbar\omega=92$ eV. Peak B (p-like), approaching the Fermi level around 64 eV, diminishes then to 2.9 eV below E_F for $\hbar\omega=110$ eV. Peak C (s-like) has the lowest value of the binding energy at point Γ (-11.4 eV) for $\hbar\omega$ around 60 eV and disperses along direction X (ΓKX line) with the value of the binding energy at X equal to -6.8 eV for $\hbar\omega=110$ eV. For $\hbar\omega=70$ eV down to 35 eV, two satellite structures, C' and D, appear, whose only structure C' shows a slight dispersive behavior; in effect peaks A, B, and D practically present no dispersion between 35 and 62 eV.

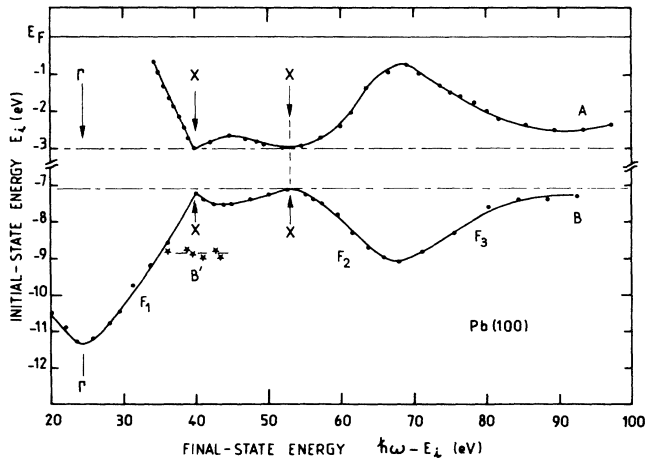

FIG. 3. Measured initial-state energy vs final-state energy: $E_f=\hbar\omega-|E_i|$, for Pb(100). The position of high-symmetry critical points Γ and X is indicated for peaks A and B.

Figure 6 shows the normal-emission spectra of the p bands taken at low photon energy (the range 9–20 eV); we can notice that peaks A and B are much better resolved than the corresponding structures observed at higher photon energy: peak A presents a minimum at 1.1 eV below E_F for $\hbar\omega=14.5$ eV, and approaches E_F for $\hbar\omega=10$ eV and also towards $\hbar\omega=18.5$ eV. In the low-energy-photon range we also follow the dispersion of peak B, which has a relative minimum of the initial-state energy at 3.35 eV below E_F for $\hbar\omega=10-10.5$ eV. The photoemission peak corresponding to the s band can be observed in the low-photon-energy spectra around $\hbar\omega=15$ eV (see Fig. 1 of Ref. 17). The binding energy of this peak is 6.85 eV below E_F.

The dispersion curves shown in Fig. 7 give the variation of the initial-state energy E_i versus final-state energy $E_f=\hbar\omega-|E_i|$ for all the observed structures. From this diagram, one observes that peaks B and C have a symmetrical behavior and correspond to a same final-state band, which starts at $E_f=42$ eV (Γ point) and ends at E_f around 110 eV (X point). Also, by considering the final-state energy at which peak A shows the strongest dispersion (around the K point), one finds that the dispersion of this final state is well described by the shift of the free-electron parabola

$$E_f=\hbar^2(k_\perp+G_{220})^2/2m^*+V_0 \tag{1b}$$

with $V_0=-11.4$ eV and $m^*=0.91m$. This value of the effective mass is rather approximate because of the lower accuracy with which we can locate the high-symmetry points Γ and X.

Now, by reconsidering the photoelectron spectra as a

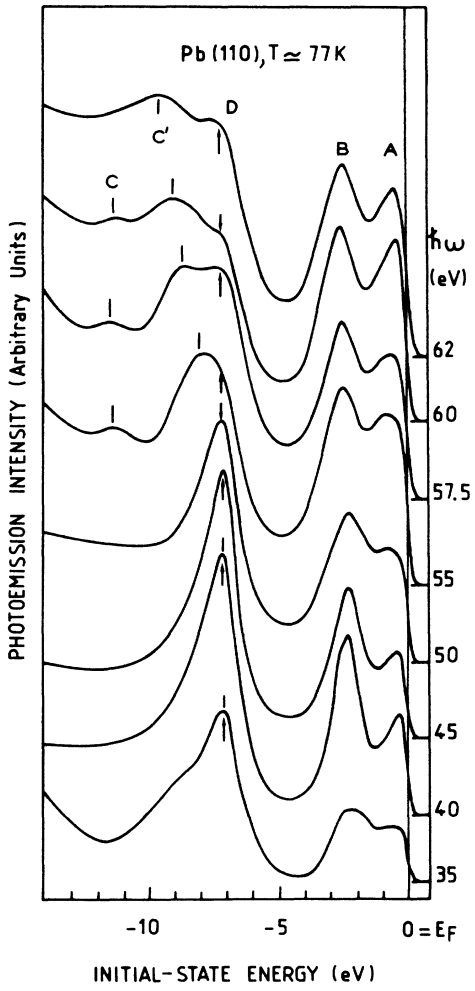

FIG. 4. Angle-resolved photoelectron spectra from Pb(110) at 77 K, recorded in normal emission with photon energy between 35 and 62 eV. The behavior of peaks (C,C') and D is described in the text. Arrows indicate indirect transitions (D structure).

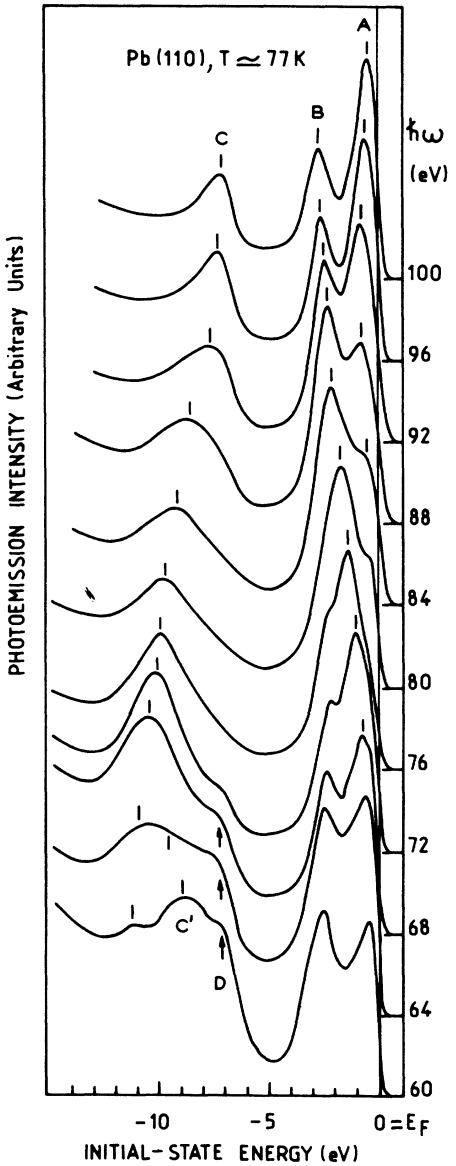

FIG. 5. Angle-resolved photoelectron spectra from Pb(110) at 77 K, recorded in normal emission with photon energy between 60 and 100 eV. Arrows indicate indirect transitions (D structure).

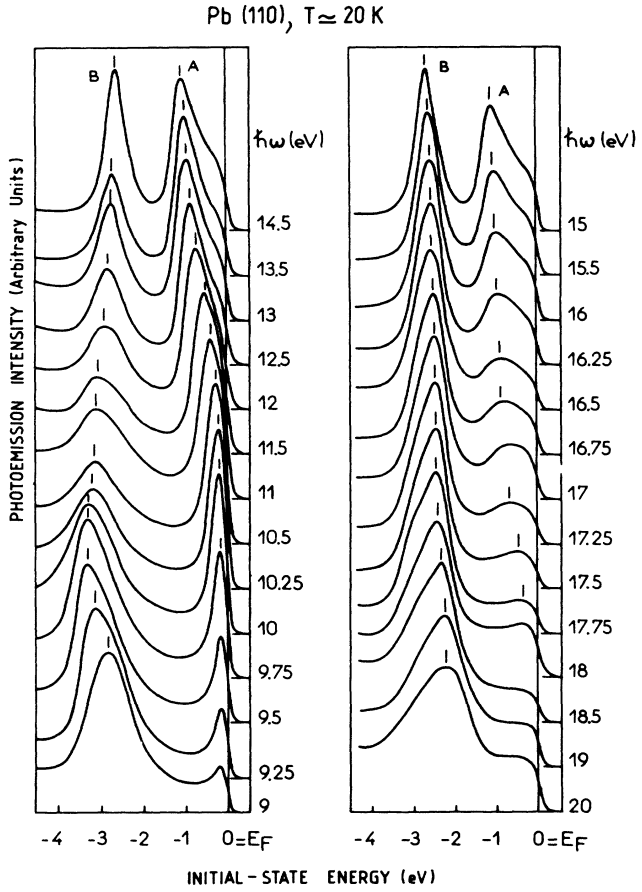

FIG. 6. Normal-emission photoelectron spectra from Pb(110) at 20 K for photon energy $\hbar\omega$ between 9 and 20 eV.

TABLE I. Binding energies for the valence bands of s- and p-like symmetry at the X point.

Valence band	Pb face	Binding energy at the X point (eV)]/E_F	Photon energy (eV)
s band	(100)	-7.15 ± 0.05	60
	(110)	-6.80 ± 0.1	120
	(110)	-6.85 ± 0.05	15
p band	(100)	-3.00 ± 0.05	55
	(110)	-2.90 ± 0.1	110
	(110)	-3.35 ± 0.03	10

function of the photon energy shown in Figs. 1, 2, and 4–6 and the experimental initial-state dispersion curves displayed in Figs. 3 and 7, one can summarize the main results, for lead, as follows.

(i) The bottom of the s band at the Γ point is located around 11.4 below the Fermi level both for face (100) and face (110).

(ii) The binding energies for the valence bands of s- and p-like symmetry at the X point are shown in Table I: a discrepancy of about 0.35 eV is found when one considers the results obtained at high [(100) face] and low [(110) face] photon energies, i.e., -7.15 versus -6.85 eV for the s band and -3.00 versus -3.35 eV for the p band. However, the binding energies for the s band at the X point on the face (110) (ΓKX direction) obtained at high (-6.8 eV) or low (-6.85 eV) photon energy are in fine agreement.

(iii) The binding energy around K of the higher p band determined at high photon energy is -0.8 eV, while it is -1.1 eV if determined for low-energy incident photons

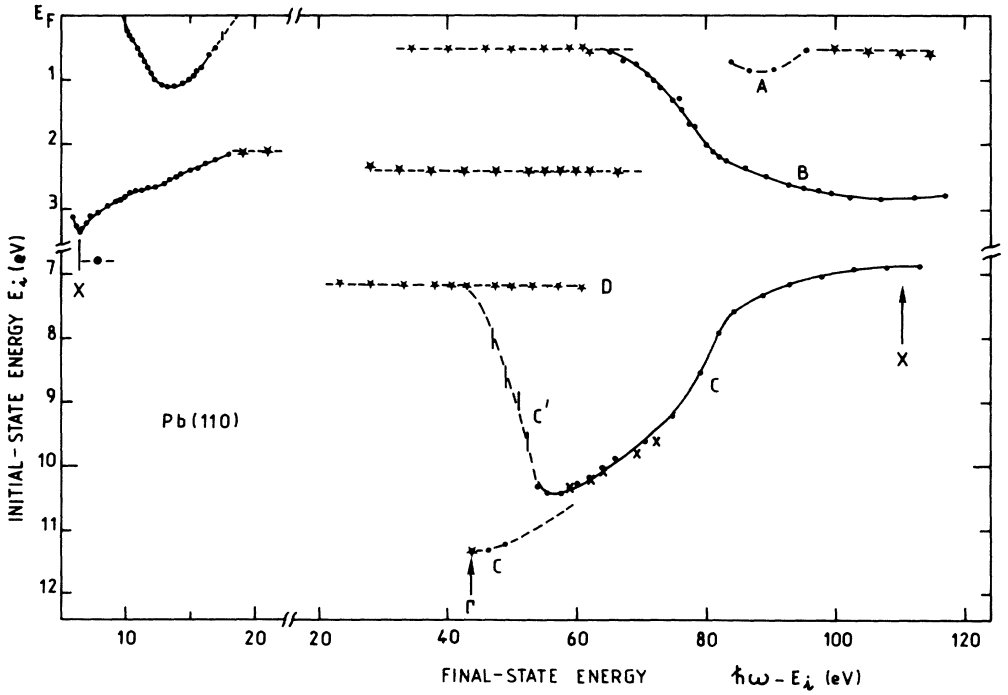

FIG. 7. Measured initial-state energy vs final-state energy, $E_f=\hbar\omega-|E_i|$, for Pb(110). The Γ and X critical point positions are also indicated for peaks A, B, and C.

TABLE II. Binding energy (eV) of lead at different high-symmetry points of the Brillouin zone.

	Γ	X		K		
		s band	p band	s band	p band	p band
Experimental results	−11.4	−6.80	−3.35	−6.90	−2.65	−1.0
Loucks (Ref. 12) RAPW, not self-consistent	−11.25	−6.70	−3.55	−6.70	−2.75	−1.20
Zdetsis *et al.* (Ref. 33) APW, partly relativistic, self-consistent	−12.4	−7.6	−3.1	−7.8	spin-orbit coupling not included	
Sommers *et al.*, (Ref. 34) KKR relativistic, self-consistent	−11.45	−6.15	−3.0	−6.15	−2.35	−0.85
Looney and Dreesen (Ref. 35) KKR, relativistic, self-consistent	−12.50	−6.60	−3.90	−6.60	−3.00	−1.65
Horn *et al.* (Ref. 11) LRC, relativistic, self-consistent	−11.66	-6.78	−3.37	−6.82	−2.67	−1.09
Anderson *et al.* (Ref. 13) pseudopotential	−9.8	−5.2	−3.40			
McFeely *et al.* (Ref. 14) LCAO	−11.9	−6.8	−3.0	−6.8	−2.1	−0.75

(see Fig. 7) on the same surface.

Thus, the results shown in Figs. 1–7 and summarized in Table I present some discrepancies in the values of the measured binding energies at high-symmetry points (particularly at the X point) and, further, photoemission profiles modify their shape for different photon energy. These differences can be partially eliminated and understood by taking into account the effect of the mean free path of the photoexcited electrons. The figures of Table I are determined within the framework of the direct-transition model, which assumes the conservation of the wave vector during the photoemission process. Now it is known that the direct-transition model for photoemission is quite a good approximation when the electron mean free path L remains much larger than $a_\perp$, the distance between two successive layers of atoms parallel to the surface. However, band-structure measurements at normal-emission are made in a wide photon-energy range (typically 30–100 eV) and thus L can get values of about 4–5 Å.[18] For such low values of L, the conservation rule of the normal component of the wave vector $K_\perp$ during the photoemission process is no longer valid so that the observed spectra are affected by the contribution of non-direct transitions through the sum on the initial states. So the direct-transitions model must be be improved by considering the influence of the inelastic scattering of the photoexcited electrons in final states. For example, the valence-band dispersion for Pb(100) is rather strong in the vicinity of the X point: this implies asymmetrical experimental profiles and great shifts of the observed peaks with respect to the energy positions expected within the framework of the direct-transition model. Instead, the valence-band dispersion is rather weak along the symmetry direction ΓKX (with the exception of the second p band, the closest to the Fermi level) and nonexistent for the s band between K and X, drastically reducing the effect of indirect transition in the normal-emission spectra from the (110) surface. The mean-free-path effect is of course negligible for low energies, where the photoelectron escape depth becomes by far larger.[18]

In conclusion, the binding energies at the point X for the s band (lowest) and p bands deduced from intermediate and low photon energies are not in good agreement. The main reason for this discrepancy can be attributed to the role of the photoexcited mean free path, which challenges the criterion $L \gg a_\perp$.

In the next section the influence of nondirect contributions to the angular-resolved photoemission spectra of lead, that is the effect of non-k-conserving transitions, will be discussed within the framework of a simplified model of photoemission.

IV. EFFECTS OF QUASIPARTICLE LIFETIME

The photoemitted elastic current per elementary solid angle $d\Omega$ (direction $\mathbf{R}$) and with kinetic energy between E and $E+dE$ can be written[19–21]

$$\frac{d^2I(\mathbf{R};E,\omega)}{d\Omega\, dE} = AE^{1/2}\int d^3r \int d^3r'\, \psi_L^*(\mathbf{r},\mathbf{R};E)H_{\text{int}}(\mathbf{r}) \times[G^+(\mathbf{r},\mathbf{r}';E-\hbar\omega+\phi)/2\pi i] \times H_{\text{int}}(\mathbf{r}')\psi_L(\mathbf{r}',\mathbf{R};E)\,, \quad (2)$$

where ψ_L^* is the time-reversed low-energy electron-diffraction type final state, H_{int} is the interaction Hamiltonian between the photon field and the electrons, and G^+ is the nonlocal occupied density of states. G^+ can be projected on the occupied one- particle states $\psi_{\mathbf{k}_v}$:[20]

$$\frac{1}{2\pi i}G^+(\mathbf{r},\mathbf{r}';E-\hbar\omega+\phi) = \int d^3k_v\,\psi_{\mathbf{k}_v}^*(\mathbf{r}')A_{\mathbf{k}_v}(E-\hbar\omega+\phi)\psi_{\mathbf{k}_v}(\mathbf{r}),$$

where $A_{\mathbf{k}_v}(E-\hbar\omega+\phi)$ is the hole spectral function. Then, Eq. (2) is rewritten as

$$\frac{d^2I(\mathbf{R};E,\omega)}{d\Omega dE} = AE^{1/2}\sum_{\mathbf{k}_v} A_{\mathbf{k}_v}(E-\hbar\omega+\phi)\left|\int d^3r\,\psi_L^*(\mathbf{r},\mathbf{R};E)H_{\text{int}}(\mathbf{r})\psi_{\mathbf{r}_v}(\mathbf{r})\right|^2. \tag{3}$$

We restrict our discussion to normal-emission spectra and sufficiently high photon energies such that (i) the final-state wave function can be represented by one Bloch wave $\phi_{\mathbf{k}_f}$ and (ii) one can neglect photoemission induced by the potential step from vacuum to the crystal ("surface photoemission," non-$k_\perp$-conserving) and thus interference between bulk and surface terms in Eq. (3). This surface contribution is included in the detailed calculation of the angle-resolved photoemission spectra of Na by Shung and Mahan[22,23] and they conclude that its relative weight decreases as the photon energy increases. Moreover, for lead, this surface contribution is already very small at low photon energies (as deduced from the comparison of yield measurements made with p-and s-polarized light).

Then, Eq. (3) can be rewritten as

$$\frac{d^2I(\mathbf{R};E,\omega)}{d\Omega\,dE} = AE^{1/2}\sum_l\sum_{\mathbf{k}_i^l} A_{\mathbf{k}_i^l}(E-\hbar\omega+\phi)|t_{\mathbf{k}_f}|^2\left|\int d^3r\,\phi_{\mathbf{k}_f^l}^*(\mathbf{r},\mathbf{R};E)H_{\text{int}}(\mathbf{r})\phi_{\mathbf{k}_i^l}(\mathbf{r})\right|^2, \tag{4}$$

where $\phi_{\mathbf{k}_f^l}$ and $\phi_{\mathbf{k}_i^l}$ are Bloch waves, l is the band index, $\mathbf{k}_i^l$ is the initial-state wave vector in band l, and $t_{\mathbf{k}_f}$ is the transmission coefficient of the Bloch wave $\phi_{\mathbf{k}_f}$ in vacuum. The matrix element

$$|M_{fi}^l|^2 = \left|\int d^3r\,\phi_{\mathbf{k}_f^l}^*(\mathbf{r},\mathbf{R};E)H_{\text{int}}(\mathbf{r})\phi_{\mathbf{k}_i^l}(\mathbf{r})\right|^2 \tag{4'}$$

can be treated according to the method first developed by Mahan (19) in order to give the condition of validity of a model for direct transitions, when inelastic scattering in the final state is taken into account. Mahan suggests giving k_f a complex value $k_f+\frac{1}{2}i/L$.

The matrix element M_{fi}^l is then calculated over the elementary unit cell and summed over the atomic sites l. The sum over a plane parallel to the crystal surface gives conservation of the parallel wave-vector component, whereas the sum made for the wave-vector component perpendicular to the crystal surface introduces the expression $f(\Delta k_\perp)$:

$$f(\Delta k_\perp) = [1+\exp(-a_\perp/L)-2\exp(-a_\perp/2L)\cos(a_\perp\Delta k_\perp)]^{-1},$$

where $a_\perp$ is the distance between two successive layers parallel to the surface.

Equation (4) can be rewritten as

$$\frac{d^2I(\mathbf{R};E,\omega)}{d\Omega\,dE} = AE^{1/2}\sum_l\sum_{\mathbf{k}_i^l} A_{\mathbf{k}_i^l}(E-\hbar\omega+\phi)f(\Delta k_\perp)|t_{\mathbf{k}_f}|^2|M_{fi}^l|^2\delta(\mathbf{k}_{i\parallel}-\mathbf{k}_{f\parallel}) \tag{5}$$

with $|M_{fi}^l|^2$ calculated over the elementary unit cell.

The function $f(\Delta k_\perp)$, where $\Delta k_\perp = \text{Re}(k_{f\perp}-k_{i\perp})$, gives the relaxation of the conservation rule for the perpendicular component of the momentum.[24]

This function is represented in Fig. 8, together with the initial- and final-state dispersions for a direct transition in the middle of the initial-state band Δ_1 (p symmetry) and a value of $L=4.5$ Å. We can note that over the range of variation of Δ_1 the function $F(\Delta k_\perp)$ keeps about half of its maximum value, which shows the spread of allowed $k_\perp$ values.

Photoemission curves have been calculated by means of Eq. (5) for Pb(100) and final-state energies between 52.5 and 67.5 eV above E_f using a constant matrix element and transmission coefficient (for a given $\hbar\omega$ and initial-state band). This particular range of photon energy is chosen so that (i) the final state can be described by a free-electron-like state and (ii) the range of energy covers the dispersion of the p bands (see Fig. 3).

The hole-spectra function was approximated by a Lorentzian normalized to unit surface:

$$A_{\mathbf{k}_i^l}(E-\hbar\omega+\phi) = \begin{cases} \dfrac{\Gamma_i^l(E_i)}{1+\left|\dfrac{E-E_i(k_i^l)-\hbar\omega+\phi}{\Gamma_i^l(E_i)}\right|^2}, & E_i<E_F \\ 0, & E_i>E_F \end{cases}$$

with $\Gamma_i^l(E_i)=\beta^l(E_i-E_F)^2$ indicating the inverse hole lifetime. The dispersion of the final state was described by a quasi-free-electron parabola

$$E_f = \hbar^2(k_{i\perp} - G_{002})^2/2m^* + V_0 \quad (6)$$

with $m^* = 0.88m$ and $V_0 = -11.4$ eV. For the dispersion of the initial states, we started with Loucks calculated band structure[12] and modified it by trial and error until self-consistency with the experimentally determined points was reached (see discussion of Fig. 10 below).

The calculated curves are represented in Fig. 9 by solid lines ($L = 4.5$ Å; $\beta' = 9\times10^{-3}$ eV^{-1} for the s band and 3×10^{-2} eV^{-1} for the p band) while the dots correspond to the experiment. The calculated spectra have been convolved with a Gaussian instrumental function of 250 meV full width at half maximum (FWHM). In this figure, the dashes indicate for every spectrum the direct-transition position ($\Delta k_\perp = 0$).

The agreement between experimental and calculated curves is very good, both for the shapes and shifts in binding energies at X point: -0.3 and -0.37 eV compared with -0.3 and -0.35 eV as deduced from low-energy data. Moreover, the values obtained for the FWHM of the hole spectral function at $X(2\Gamma_i)$, 0.6 eV for the p band and 0.9 eV for the s band, are very close to the values obtained from the low-energy spectra [(110) face] at corresponding initial-state energies, (1.1±0.2 eV for the s band ($\hbar\omega = 15$ eV) and 0.6±0.05 eV for the p band ($\hbar\omega = 14$ eV). The parabolic variation for the hole inverse lifetime fits also very well with the data shown by Levinson for aluminum and zinc (see Fig. 19 of Ref. 5).

The value obtained for L, 4.5 Å, seems reasonable owing to the kinetic energy of the photoelectrons but it must be pointed out that this parameter is the most sensitive to the approximations we have made (e.g., constant matrix element).

Figure 10 shows the energy dispersion of bands s and p as input in the calculation which gives the best fit both with the calculated spectra (solid lines in Fig. 9) and with the values corresponding for each spectra to the direct transition ($\Delta k_\perp = 0$, rectangles in the figure). The dots, with dashes representing the experimental uncertainty, are deduced directly from the experimental spectra by using the direct-transition model. The dispersion of the s band (Δ_1) corresponds to the theoretical one[12] rigidly shifted downwards by 150 meV. The p band crosses the Fermi level for a $k_\perp$ value in nice agreement with the Fermi-surface results obtained by Anderson *et al.*[25] (de Haas–van Alphen effect) and Stedman *et al.*[26] (Kohn anomaly).

As far as the face (110) of lead is concerned, in the photon energy range 70–100 eV, the photoemission profiles are also well reproduced by using this model and show

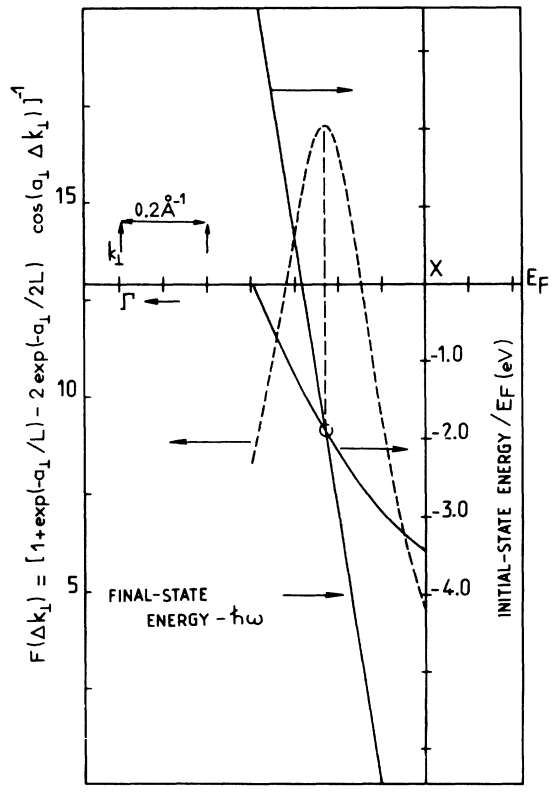

FIG. 8. Dispersion of initial and final band states along the ΓX direction. The function $F(\Delta K_\perp)$ defines the relaxation of the $K_\perp$ conservation during the photoexcitation process. Note that the function $F(\Delta K_\perp)$ keeps about half of its maximum value, in the range of dispersion of the initial states.

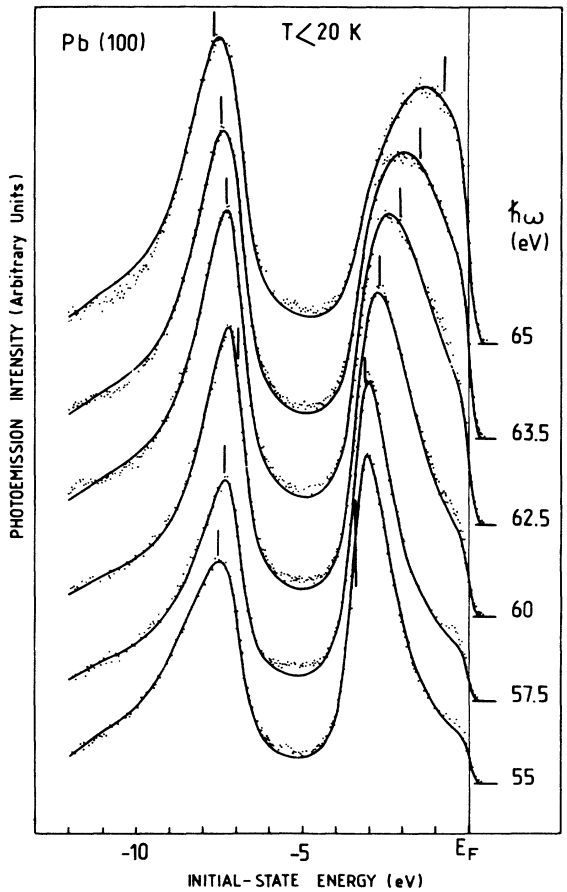

FIG. 9. Comparison between experimental data (dots) and calculated spectra obtained by consideration of inelastic scattering (solid lines). The dashes indicate for every spectrum the direct-transition position ($\Delta k_\perp = 0$).

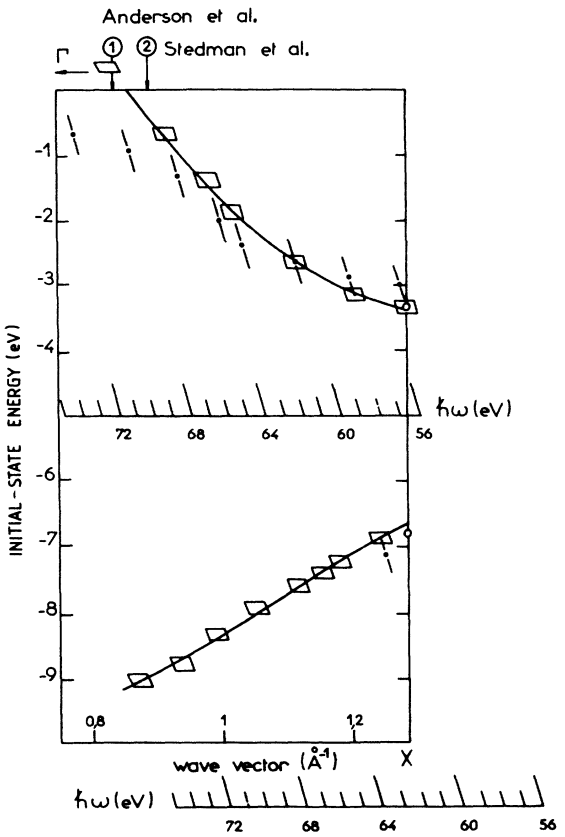

FIG. 10. Experimental dispersion of lead energy bands along the ΓX direction. Dots are obtained by simply using the direct-transition model, while squares and solid lines result from the fit of the experimental spectra to Eq. (4).

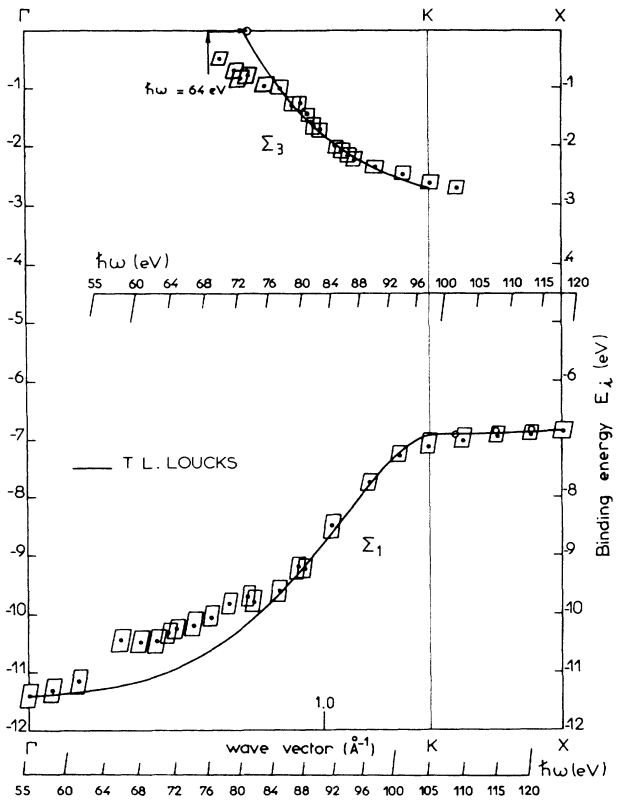

FIG. 11. Comparison between experimental (rectangles) and calculated (solid line) (Loucks, Ref. 12) valence-band dispersions of $\Sigma_3(p)$ and $\Sigma_1(s)$ bands.

that the error introduced by using the direct-transition model is always less than 100 meV. This is well understood by considering that (i) the band dispersion along the ΓKX line is much weaker than along the X direction and (ii) the group velocities in the initial and final states are in this case of opposite signs.

V. EXPERIMENTAL DISPERSION CURVES VERSUS BAND-STRUCTURE CALCULATIONS

A. Experimental valence-band structure along the ΓKX line

The position of photoemission peaks shown in Sec. III gives the basic experimental information for the valence-band structure to be compared with the theoretical energy versus momentum dispersion curves. Figure 11 shows the experimental results for the Σ_1 (s band) and Σ_3 (lower p band) bands along ΓKX. The experimental points are obtained from Fig. 7, which gives final versus initial energy for a given peak, and from Eq. (1b), which connects the final-state energy to the wave vector $k_\perp$. The comparsion of the experimental valence-band structure with the theoretical structure obtained by Loucks[12] with a RAPW calculation (solid line in Fig. 11) shows a fine agreement apart from the interval of $k_\perp$ values between 0.25 and 0.7Å^{-1}, where the experimental points lie outside the calculated curves both for Σ_3 and Σ_1 bands. The experimental dispersion of the uppermost p band (Σ_1 symmetry in single group notation) could also be obtained from high-energy-photon measurements, but these results are much affected by the low instrumental resolution and the contribution of indirect transitions. For these reasons, we prefer to use the low-energy-photon ($\hbar\omega < 20$ eV) and low-temperature ($T < 20$ K) spectra, which are more precise, but require a knowledge of the final-state dispersion. The band calculation by Horn *et al.*[11] presents the electronic structure up to 30 eV above E_F: his results along ΓX and ΓKX symmetry lines (see Fig. 12) give us the necessary information about the band behavior. In this case the final-state band useful for the low-energy photoemission results ($9 \leq \hbar\omega < 20$ eV) is identified as f_1 in Fig. 12.

The same final state f_1 is represented by a solid line in Fig. 13 (upper part), whereas the experimental valence band of Σ_3 symmetry, deduced from high-energy measurements, is denoted by squares in the lower part of the figure. The experimental final state at the X point is observed at 6.5 eV above E_F (see Fig. 7): this requires a downward shift of the calculated band f_1 by about 0.5 eV at X. The calculated band needs only to be slightly distorted in order to reach a good agreement between the experimental dispersion of the Σ_3 band determined from high-energy spectra (squares) and low-energy spectra (cir-

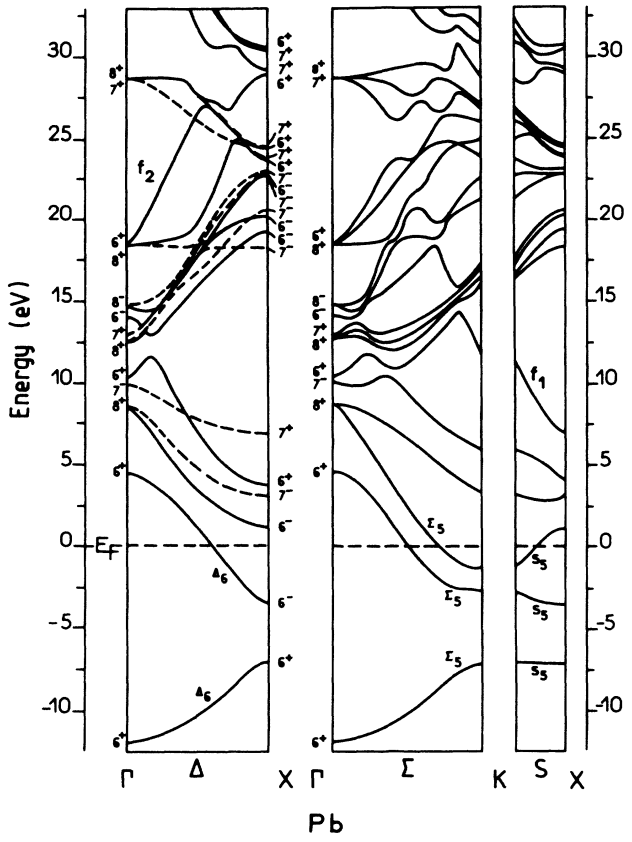

FIG. 12. Self-consistent relativistic band structure for Pb along ΓX and ΓKX high-symmetry directions of the Brillouin zone. Valence bands $\Delta_6(\Gamma X)$, $\Sigma_5(\Gamma K)$, and $S_5(KX)$ have been tested experimentally. The dispersion of final states f_1 and f_2 has been also checked.

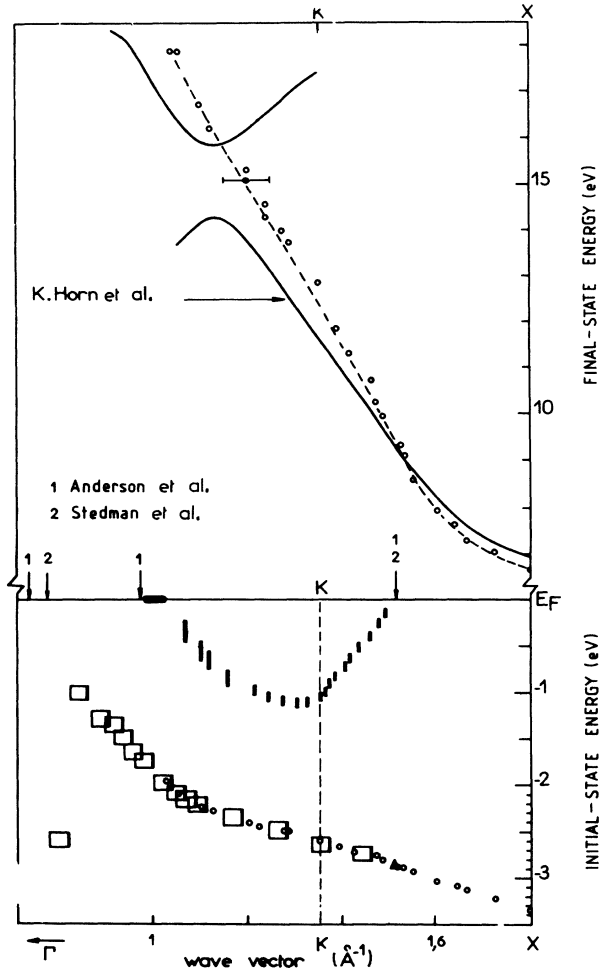

FIG. 13. Experimental dispersion of valence bands Σ_1 and Σ_3. In the upper part of the figure a comparison with the theoretical calculation of the final state f_1 is shown (Horn *et al.*, Ref. 12).

cles). However, the photoemission data (open circles) "close" the forbidden gap of the one-electron band calculation for the final state. Once one obtains the measured final-state dispersion (circles in the upper part of Fig. 13), the experimental dispersion for the Σ_1 band (uppermost p band) as a function of $k_\perp$ is easily obtained starting from the corresponding curves of Figs. 6 and 7.

The intersection with the Fermi level for $k_\perp = 1$ and 1.5Å^{-1} is again in fine agreement with the results reported by Anderson *et al.*[25] and Stedman *et al.*[26] obtained by different experimental techniques.

In conclusion, we have listed in Table II the values of the binding energy for lead at points of high symmetry obtained from various sources and our photoemission results in order to make a comparison between theory and experiment. First, the experimental data are in best agreement with the band results given by Loucks[12] and Horn.[11] The difference in the value of the binding energy at Γ is small compared with the measured value ($E_{(L)}^{\text{theor}} = -11.25$ eV and $E_{(H)}^{\text{theor}} = -11.6$ eV versus $E_b^{\text{expt}} = -11.4$ eV, respectively). The experimental figure is in between the theoretical values and the discrepancy with the calculated value might also be due to the difficulty of observing the bottom of the s band.

The agreement is still good with the results of Anderson *et al.*,[13] if one displaces the s band rigidly downwards by 1.8 eV. This shift is justifiable by considering the Darwin correction and the mass-velocity effects which shift the s band from the p band almost in a rigid way and were neglected in this calculation.

B. Experimental final-state dispersion

Once the experimental and theoretical dispersions for the initial-state bands are seen to be in good agreement, one can use the data to describe the final state's dispersion both for face (100) and face (110) in the interval of energy between 22.5 and 85.5 eV and 35 and 110 eV, respectively (see Figs. 14 and 15).

Figure 14 shows the dispersion of the final states F_1, F_2, and F_3 observed in normal photoemission for Pb(100) along the ΓX direction. The experimental dispersion (rectangles and squares in the figure) from Γ_1 at 22.5 eV above E_F towards X_1 (in fact, between X_4' and X_1), is not free-electron-like. When it is compared with the band calculation due to Horn *et al.*[11] (band f_2 in Fig. 12) one finds a good agreement for $0 < k_\perp < 0.75$ Å^{-1}, if the cal-

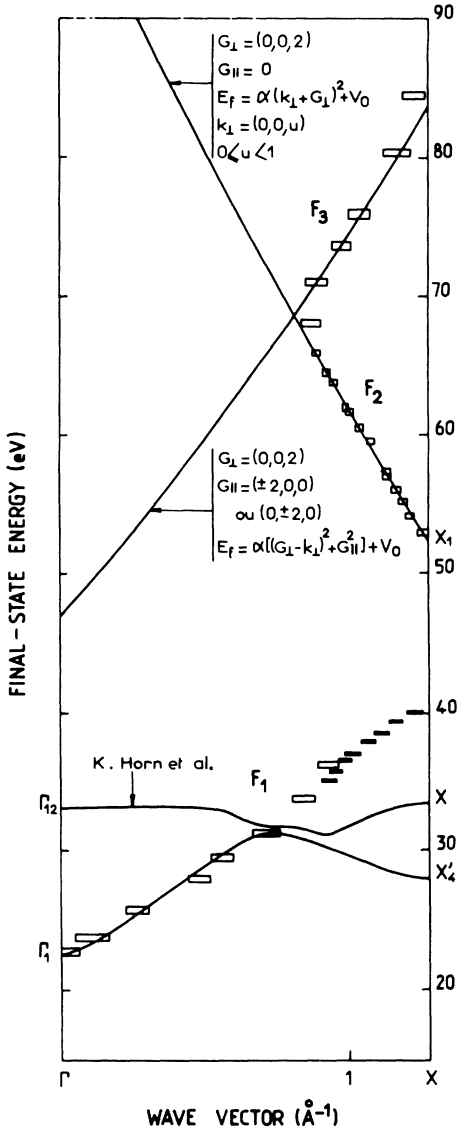

FIG. 14. Final states along the ΓX direction observed in normal photoemission for Pb(100) between 20 and 85 eV above E_F.

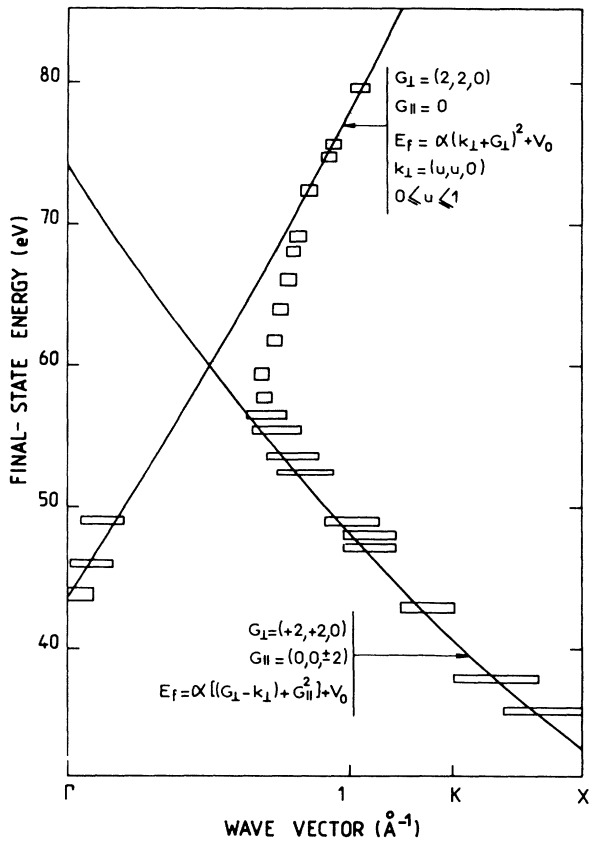

FIG. 15. Final states along the ΓKX direction observed in normal photoemission for Pb(110) between 45 and 80 eV above the Fermi level.

culated band f_2 (Fig. 12) is rigidly displaced upwards by 4 eV: this theoretical band is derived from the principal free-electron state which is proportional to $(G_{002}-k_{i\perp})^2$. For energies higher than 35 eV, which is the superior limit of Horn's calculation for the final states, we can try to compare our photoemission results with the band results obtained for Al (up to 80 eV) by Hoffstein and Boudreaux[27] (see Fig. 6 of Ref. 29). This comparison shows that the photoemission final state F_1 reaches the zone edge at X_1, the point located midway between the points X_4' (28 eV) and X_1 (52 eV) at energy of 40 eV. The experimental results in the region of energy between 40 and 52 are too close to the zone edge (X point) and the dispersion of the final state is not clearly defined.

In the energy range from 52 to 68 eV above E_F, the photoemission curve $F2$ follows the principal free-electron state of Pb:

$$E_f=\hbar^2(k_{i\perp}-G_{002})^2/2m^*+V_0$$

(energy referred to E_F)

with $m^*0.88m$ and $V_0=-11.4$ eV, or equivalently,

$$E_f=\hbar^2/2m(k_{i\perp}-G_{002})^2+V_0^* \quad \text{with } V_0^*=-4 \text{ eV} .$$

This value of V_0^* (or m^*) corresponds to an upward shift of the empty lattice bands of the order of 5–6 eV (the free-electron Fermi energy is 9.4 eV). Finally, between 70 and 85 eV above E_F, the final-state dispersion (corresponding to the $F3$ curve) follows the relation

$$E_f=\hbar^2/2m^*[(k_{i\perp}-G_{002})^2+G_{\parallel}^2]+V_0 ,$$

with $G_{\parallel}=(\pm2,0,0)$ or $(0,\pm2,0)$, a slightly smaller value of m^*/m (0.86), and $V_0=-11.4$ eV. This final state is still free electron-like, but with an umklapp included.

Figure 5 presents the photoemission results for normal photoemission from the Pb(110) surface, along the ΓKX direction. The final state which is checked in photoemission is the principal free-electron final state

$$E_f=\alpha(k_{i\perp}+G_{\perp})^2+V_0$$

with $G_{\perp}=(220)$ and an energy shift upwards of the same order of magnitude as that for face (100). The final state measured by following the shift of the photoemission

structure C' (see Fig. 7) is still identified as an umklapp state

$$E_f = \alpha[(G_\perp - k_{i\perp})^2 + G_\parallel^2] + V_0$$

with $G_\perp = (220)$ and $G_\parallel = (00\pm 2)$ and also an upward energy shift similar to the one of the preceding umklapp. Between 60 and 70 eV over E_F, the final state is distorted with respect to the free-electron parabola: this is the origin of the discrepancy for the initial states observed in Fig. 11.

We have also observed in Fig. 14 that the comparison between experiment and theory[11] is rather good between 6.5 and 18 eV, except for the gap closing observed between 14.3 and 16 eV over E_f, due to the influence of the imaginary part of the optical potential.

So the effects of the lifetime of the photoexcited electrons, such as the closing up of forbidden gaps and predominance of free-electron-like final states,[28] are also observed in the case of lead. We have shown in Figs. 14 and 15 that the final-state bands must be displaced in order to reach an agreement with Horn's calculations, that is of 4 eV in the range 22–30 eV, or of 5–6 eV with regard to the free-electron state, starting from 50 eV. Shifts of the same order of magnitude were observed for other metals, such as Au(111) in normal photoemission,[4] Au(100),[29] Cu(111),[30] and Pd(111).[31] Such displacements are best interpreted in terms of the variation of the real part of the exchange-correlation potential for the excited states as a function of the energy of the final states.

In this context, Nilsson and Larsson[32] have reduced the disagreement observed in Cu(111) by a factor of 2 by using in their calculations the excitation potential obtained by Hedin and Lundqvist.[16] Self-energy shifts in the final state have also been demonstrated in the case of Na by Shung, Sernelius, and Mahan.[22]

VI. CONCLUSIONS

By means of low-temperature photoemission with synchrotron radiation we have measured the occupied and unoccupied band state dispersion of crystalline lead with high accuracy. The experimental valence bands present an exemplary agreement with relativistic band calculations both for energy dispersions and for binding-energy determination at Γ and X high-symmetry points of the Brillouin zone (average error less than 0.1 eV) at X. The agreement is also fine when the band structure is strongly affected by spin-orbit interaction, e.g. along the ΓKX symmetry line.[11] The simplicity of the valence-band structure, together with its accurate experimental determination, helped the analysis of final-state dispersion observed in photoemission, well described by free-electron parabolas (umklapp included) at high photon energy.

The occurrence of momentum-nonconserving transitions affects the energy-dispersion determination especially in the case of metals with strongly dispersing valence bands [i.e., for Pb(100) along the high-symmetry line X for photon energy between 55 and 65 eV] and point out the need of overcoming in that case the direct-transition model by taking into account the short mean free path of the photoelectron and the valence hole lifetime.

ACKNOWLEDGMENTS

The manuscript was written while one of us (I.P.) was visiting the University of Rennes I. It is a pleasure for him to acknowledge the kind hospitality enjoyed at the Laboratoire de Spectroscopie du Solide. Laboratoire de Spectroscopie du Solide is Unité No. 1202 Associé au Centre National de la Recherche Scientifique (CNRS). The Dipartimento di Fisica dell'Università di Milano is affiliated with the Gruppo Nazionale di Struttura della Materia del Consiglio Nazionale delle Ricerche.

*Also at Laboratoire pour l'Utilisation du Rayonnement Electromagnétique (LURE), Université Paris–Sud, Bâtiment 209D, F-91405 Orsay CEDEX, France.

†Permanent address: Dipartimento di Fisica, Università degli studi di Milano, via Celoria 16, I-20133 Milano, Italy.

[1]J. A. Knapp, F. J. Himpsel, and D. E. Eastman, Phys. Rev. B **19**, 4952 (1979).

[2]P. Thiry, D. Chandesris, J. Lecante, C. Guillot, R. Pinchaux, and Y. Petroff, Phys. Rev. Lett. **43**, 82 (1979).

[3]R. Courths, V. Bachelier, and S. Hufner, Solid State Commun. **38**, 887 (1981).

[4]P. Heimann, H. Miosga, and H. Neddermeyer, Solid State Commun. **29**, 303 (1979).

[5]H. J. Levinson, F. Greuter, and E. W. Plummer, Phys. Rev. B **27**, 727 (1983).

[6]T. S. Chiang, J. A. Knapp, D. E. Eastman, and M. Aono, Solid State Commun. **31**, 917 (1979).

[7]F. Solal, G. Jezéquel, F. Houzay, A. Barski, and R. Pinchaux, Solid State Commun. **52**, 37 (1984).

[8]F. J. Himpsel, J. A. Knapp, and D. E. Eastman, Phys. Rev. B **19**, 2872 (1979).

[9]L. Ley, R. Pollak, S. Kowalczyk, and D. A. Shirley, Phys. Lett. **41A**, 429 (1972).

[10]C. Norris and L. Wallden, J. Phys. F **2**, 180 (1972).

[11]K. Horn, B. Reihl, A. Zartner, D. E. Eastman, K. Herman, and J. Noffke, Phys. Rev. B **30**, 1711 (1984).

[12]T. S. Loucks, Phys. Rev. Lett. **14**, 1072 (1965).

[13]J. R. Anderson and A. V. Gold, Phys. Rev. **139**, A1459 (1965).

[14]F. R. McFeely, L. Ley, S. P. Kowalczyk, and D. A. Shirley, Solid State Commun. **17**, 1415 (1975).

[15]F. J. Himpsel, D. E. Eastman, and E. E. Koch, Phys. Rev. B **24**, 1687 (1981).

[16]L. Hedin and B. I. Lundqvist, J. Phys. C **4**, 2064 (1971).

[17]G. Jézéquel, A. Barski, P. Steiner, F. Solal, P. Roubin, R. Pinchaux, and Y. Petroff, Phys. Rev. B **30**, 4833 (1984); G. Jézéquel, thèse Doctorat d'Etat, Université de Rennes I, 1984.

[18]C. R. Brundle, Surf. Sci. **48**, 99 (1975).

[19]G. D. Mahan, Phys. Rev. B **2**, 4334 (1970).

[20]C. Caroli, D. Lederer-Rosenblatt, B. Roulet, and D. Saint James, Phys. Rev. B **3**, 2452 (1975).

[21]P. J. Feibelman and D. E. Eastman, Phys. Rev. B **10**, 4932 (1974).

[22]K. W. K. Shung, Bo. E. Sernelius, and G. D. Mahan, Phys. Rev. B **36**, 4499 (1987).

[23]K. W. Shung and G. D. Mahan, Phys. Rev. B **38**, 3856 (1988).

[24]D. J. Spanjaard, D. W. Jepsen, and P. M. Marcus, Phys. Rev.

B **15**, 1728 (1977).
[25]J. R. Anderson, W. J. O'Sullivan, and J. E. Schirber, Phys. Rev. B **5**, 4683 (1972).
[26]R. Stedman, L. Almqvist, G. Nilson, and G. Raunio, Phys. Rev. **163**, 567 (1967).
[27]V. Hoffstein and D. S. Boudreaux, Phys. Rev. B **2**, 3013 (1970).
[28]E. Hora and M. Scheffler, Phys. Rev. B **29**, 692 (1984).
[29]R. Rosei, R. Lasser, N. V. Smith, and R. L. Benbow, Solid State Commun. **29**, 3 (1979).
[30]P. O. Nilsson, J. Kanski, and G. G. Larsson, Solid State Commun. **36**, 111 (1980).
[31]P. O. Nilsson, G. G. Larsson, and W. Eberhardt, Phys. Rev. B **24**, 1739 (1981).
[32]P. O. Nilsson and G. G. Larsson, Phys. Rev. B **27**, 6143 (1983).
[33]A. D. Zdetsis, D. A. Papacoustantopoulos, and E. N. Economou, J. Phys. F **10**, 1149 (1980).
[34]C. B. Sommers, G. Juras, and B. Segall, J. Phys. (Paris) Colloq. **33**, C3 (1972).
[35]W. J. Looney and J. A. Dreesen, Phys. Rev. B **20**, 3051 (1979).